

Particle Dampers—Vibration Reduction Through Distributed Dissipation Over Complex Particle Shapes



Andreas Schönle, Chandramouli Gnanasambandham, and Peter Eberhard

1 Introduction

The growing emphasis on lightweight construction has not only reduced the weight of technical systems drastically but also made them more vulnerable to unwanted vibrations. This fact combined with the growing complexity of these systems has led to a rethinking of the purpose of damping devices and has paved way for the development of new methods to dissipate the unwanted vibrational energy. Their relatively simple design and their flexible ability to dissipate energy in a wide frequency range [1] have made solid particle filled dampers a popular alternative to conventional damping devices. Moreover, unlike viscous dampers, PDs do not rely on a fixed anchor point as an impulse source, which makes it even easier to mount them on technical systems. One of the earliest applications of PDs in the context of machine tools was presented in [2]. Some of the more recent applications include damping the structural vibrations of an oscillatory saw [3], noise reduction in transmission systems [4], reducing the horizontal vibrations in wind turbine towers [5], and to reduce vibrations on circuit boards of a spacecraft [6]. Furthermore, PDs have also been used to control vibrations in combustion discharge nozzles in industrial gas turbines [7].

The process of energy dissipation in PDs is very complex, as the damping performance depends on various parameters such as the strength of the forcing function (i.e. amplitude and frequency), size and geometry of the particles, inter-particle friction, material properties of the particle themselves amongst others. PDs can be more easily put to practical use in technical applications if there is a deep understanding of the

A. Schönle · C. Gnanasambandham · P. Eberhard (✉)
Institute of Engineering and Computational Mechanics, University of Stuttgart, Pfaffenwaldring
9, 70569 Stuttgart, Germany
e-mail: peter.eberhard@itm.uni-stuttgart.de

A. Schönle
e-mail: andreas.schoenle@itm.uni-stuttgart.de

underlying dissipation mechanisms. A systematic theoretical/experimental analysis of PDs in the context of free response behavior of a cantilever beam with a PD was presented in [8]. Here, an elementary analytical model to predict the macroscopic dissipative properties of PDs is reported, which was able to predict the experiments with reasonable accuracy. A parametric model of the nonlinear damping of PDs as an equivalent viscous damper was proposed in [9]. This research could be used in order to make predictions during the early design stage. Even though these models are reasonably good in predicting the macroscopic behavior of PDs, their predictions become fallible as soon as the particle-level parameters change. This is the case when PD contents has two distinctively different materials like solid and liquid, or when the particles have complicated shapes. This motivates further research to improve the understanding and applicability of PDs. Such research is to be conducted in this project using numerical simulations and laboratory experiments. The simulations are carried out using the particle simulation programm Pasimodo [10].

1.1 Dependencies of the PD Behaviour

The dependency of PD behaviour on particle movement can be illustrated by an experiment of rather simple design. In Fig. 2, one possible experimental setup is shown. Compressing the particles through the movable container walls ensures their immobility (left). Contrary to this, particles are free to move within the container volume in the second case (right). In Fig. 1 the experimental setup is illustrated schematically. Figure 3 shows the resulting measurement curves. Both of these measurements were conducted with an initial displacement of $A_0 = 40$ mm. It can be seen in Fig. 3 that significant amounts of kinetic energy can be dissipated when

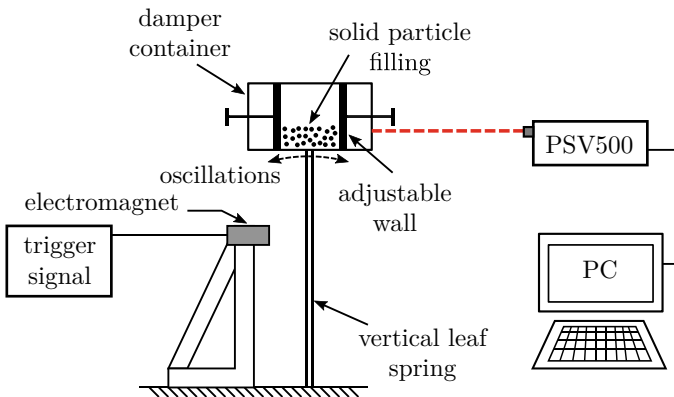


Fig. 1 Schematic view of the experimental setup used for experiments. It is to be noted that the oscillation direction is perpendicular to the acceleration due to gravity

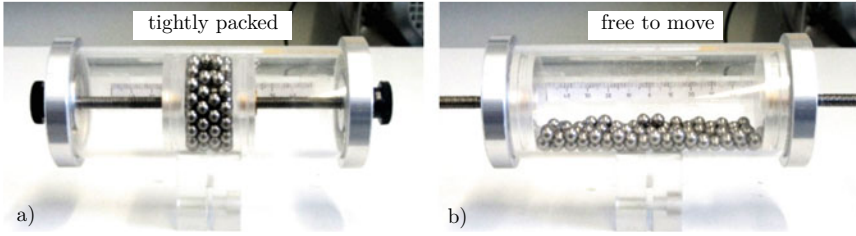


Fig. 2 The PD configurations with **a** the particles tightly packed and **b** with the particles free to move and a container length of 100 mm

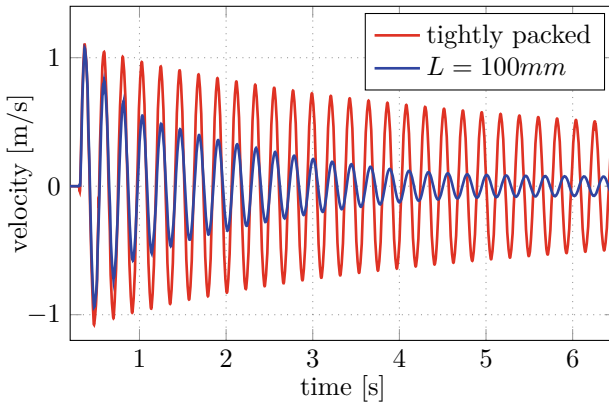


Fig. 3 Container velocities measured using an LDV for two configurations. First (red) the particles are tightly packed. Second (blue) particles are allowed to move freely. A considerable amount of kinetic energy is dissipated when particles are allowed to move freely due to inter particle collisions

the particles are allowed to move relative to each other. To quantify the dissipation present in the system, an effective decay rate parameter Λ is introduced. The decay rate during the i th cycle Λ_i is defined as the natural logarithm of two successive peak amplitudes. It is given by

$$\Lambda_i = \ln \frac{y(t_i)}{y(t_{i+1})}, \tag{1}$$

where y_i and y_{i+1} are the peak displacement of the damper container during the i th and $i+1$ th cycle, respectively. In Fig. 4, the logarithmic decay rate for each cycle Λ_i is plotted over time for both cases. Since the particles were restricted to move relative to each other in the tightly packed configuration, the dissipation in this case, seen in Fig. 4 (red line), is very small and is essentially due to the intrinsic material damping present in the leaf spring.

However, it can also be observed from Figs. 3 and 4 that a residual amplitude exists in the case of the freely moving particles. Here the amplitude of the container

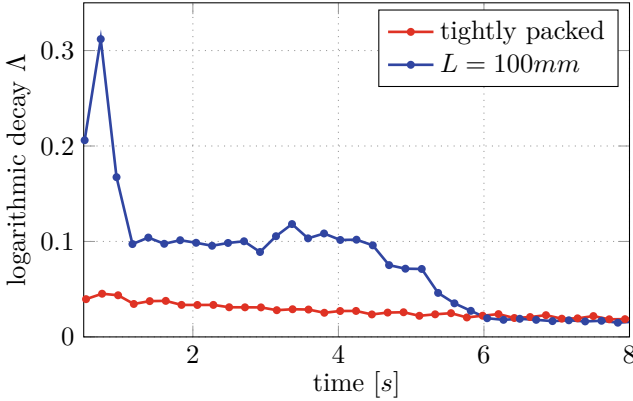


Fig. 4 The logarithmic decay Δ for both configurations. A constant decay rate, mostly due to the intrinsic material damping present in the leaf spring, is observed when the particles are tightly packed. Two distinctly different decay rates are observed when the particles are allowed to move freely

is not sufficient to keep the particles moving. Thus, hindering dissipation extending the material damping which is observed for the case of tightly packed particles. These insights give an idea for improving the overall dissipation behaviour of PDs, for a more detailed analysis see [11]. Keeping the particles in motion and finding measures to improve the dissipation for low amplitudes of excitation are, therefore, overall research objectives in this project.

Tools to grant detailed insights on how the taken measures improve the damping behaviour of PDs accelerate this process. This leads to a combined approach of numerical simulation and laboratory experiments. While the simulations offer access to the mechanisms within the PD, experiments ensure the agreement of the simulations with the actual system. A snapshot from a PD simulation with spherical particles can be seen in Fig. 5. The good agreement in Figs. 6 and 7 illustrates the feasibility of this approach for spherical particles using DEM.

2 Influence of Fillings

One possible way to increase the damping, even under low driving accelerations, is, to combine a liquid with solid fillings. Another influence factor is the shape of the particles as it alters the contact situation among particles. These influences are therefore of great interest for the overall performance of PDs.

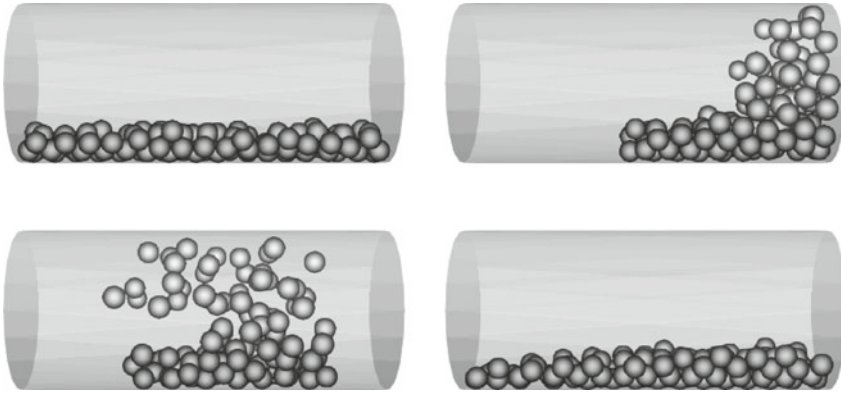


Fig. 5 DEM simulation snapshots showing the motion of the solid particles

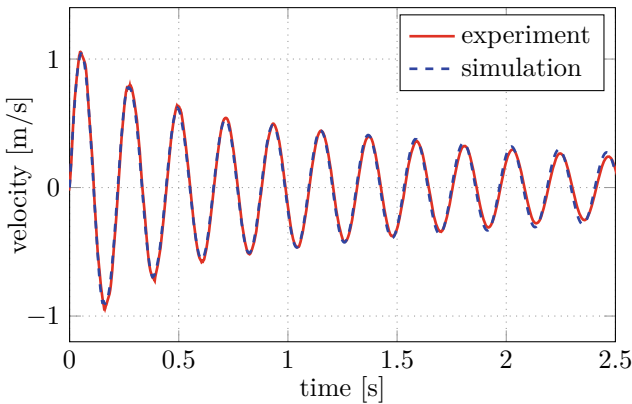


Fig. 6 Comparing DEM simulation results and experimental data for a damper filled with 100 aluminum spherical particles. A good agreement between experiment and simulation is observed

2.1 Influence of Liquid

Before investigating the effects of an added liquid, it is necessary to investigate the case where the damper is filled only with liquid contents. To simulate liquids in the PD the SPH method is used, as it is shown in [12]. The liquid motion resulting from these simulations is illustrated in Fig. 8. Figures 9 and 10 also show good agreement for this approach.

Combining solid particles with liquid in PDs has great potential in improving the damping behaviour. To study the effects of this approach the previously used simulation methods are combined. The damping behavior of a damper filled with a combination of solid particles and a liquid, as shown in Fig. 11, is investigated. Again this is done in both, numerical simulations and experiments. While the simulation

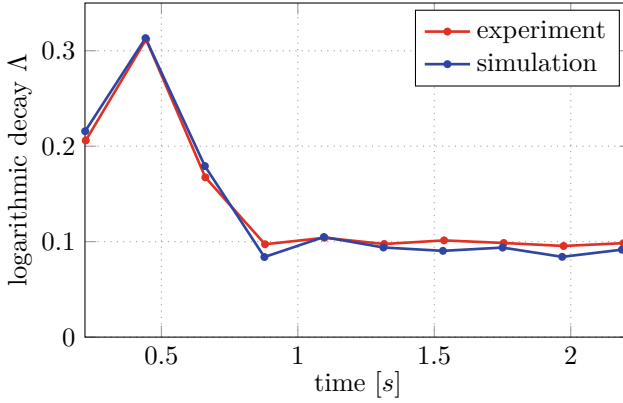


Fig. 7 Logarithmic decay rates predicted by DEM simulations and measured using experimental data for a damper filled with solid particles. Initially, due to the large relative motion, higher decay rates are observed

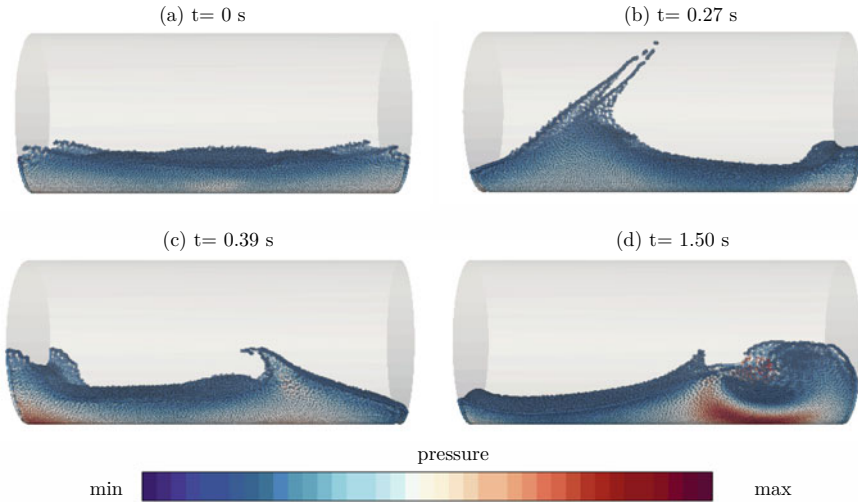


Fig. 8 SPH simulation snapshots showing the motion of the liquid modeled

grants important insights to understand the mechanisms leading to the improved damping behaviour, the experimental data is used for confirmation of the results. In the simulations the contact model is extended to cover the fluid-solid interactions. For this purpose, the damper container is filled with 100 aluminum particles and 30 ml of distilled water. In order to ensure a fair comparison between all the damper configurations, compensation masses were added during the laboratory experiments, so that all the configurations have the same static mass, measured using a weighing scale. The simulation results, showing the velocity amplitude decay for all three damper

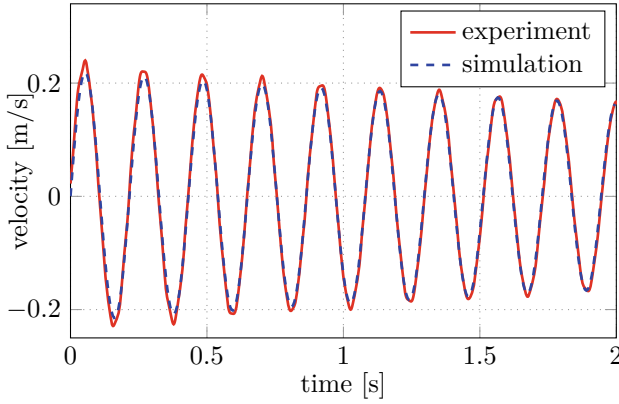


Fig. 9 Comparing SPH simulation results and experimental data for a damper filled with 30 ml distilled water. A good agreement between experiment and simulation is observed

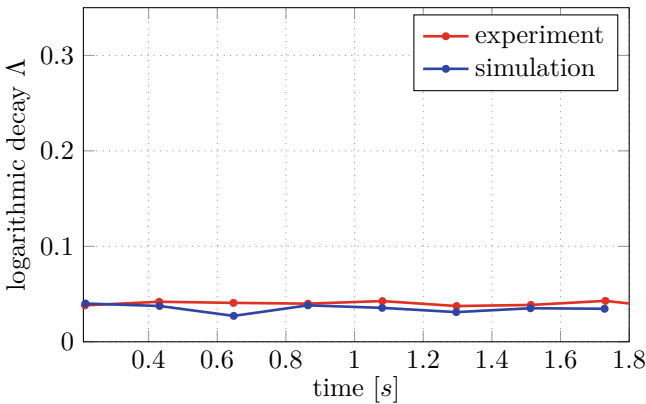


Fig. 10 Liquid filled dampers exhibit decay rates which are much smoother than for only solid particle filled dampers. Liquid filled dampers continue to dissipate energy even under low vibration amplitudes

configurations is seen in Fig. 12. As seen in an earlier investigation, the only-solid particle-filled damper seems to be not so effective under low acceleration conditions. Under low forcing condition, the solid particles seem to arrange themselves in an orderly packing. This makes it increasingly difficult for the particles to move relative to each other. As a consequence, the decay rate of solid-filled dampers in Fig. 13 (green) is observed to be lower than that of solid-liquid-filled dampers (blue). In fact, the worst performing of all three damper configurations is the one with only liquid filling. Even though there is a large relative motion observed between liquid layers, the resistance forces acting against the motion of the damper container are small, due to the lower momentum carried by the liquid.

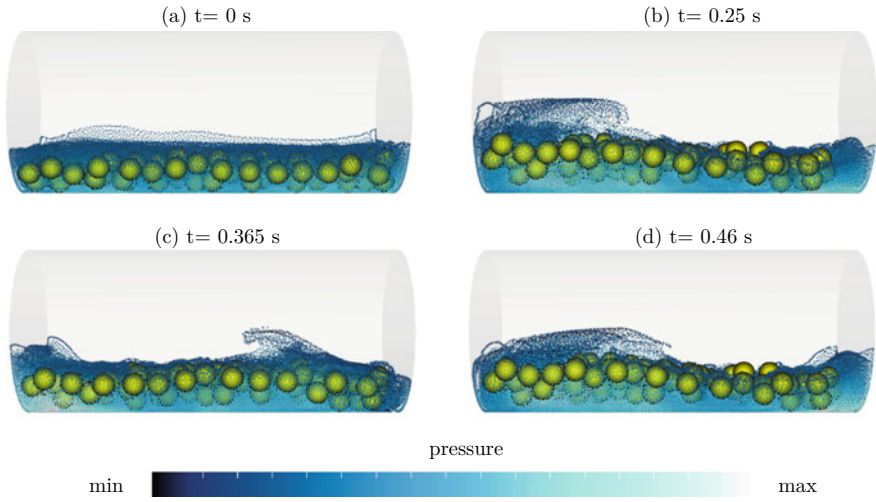


Fig. 11 Fluid-solid motion, predicted by coupled DEM-SPH simulations, at various time steps. The liquid is visualized using smaller coloured balls, whereas the solids are visualized as large yellow balls

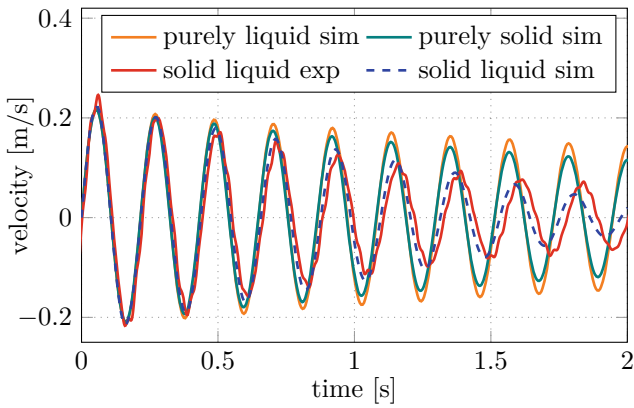


Fig. 12 The velocity of the damper container is compared for all the damper configurations. The blue dotted curve represents the container velocity predicted by coupled SPH-DEM simulations of a damper filled with solids and liquid particle

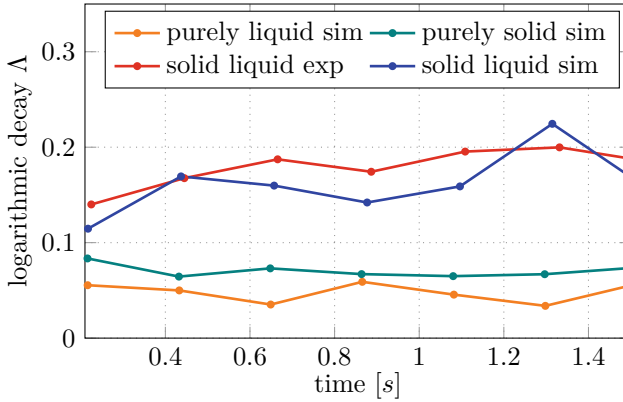


Fig. 13 Decay rates of all damper configurations are compared. Decay rates of solid filled dampers and liquid filled dampers are relatively similar. A substantial improvement in the damping performance is observed in the solid and liquid filled dampers

On the other hand, it can be seen that the damper configuration with a combination of both, solid-liquid contents indeed performs better than the other two configurations. Since the solid particles are surrounded by a liquid, it is much more difficult for the solids to remain in an ordered structure. This disorder makes them more susceptible to move relative to each other, which ultimately leads to stronger collisions and intern leads to more energy dissipation. In general, good agreement for the combined solid liquid simulation can be observed in Fig. 12. Therefore, the coupled SPH-DEM simulation is a useful tool to investigate particle dampers and the behaviour of their fillings. From Figs. 12 and 13 a significant increase in the decay of the vibration amplitude is seen.

This motivates further simulations and experiments to gain additional insights in the underlying effects resulting in such improvement. Possible influences considered are the solid-liquid fill ratio and the shape of the solid particles.

2.2 Influence of Particle Shape

The influence of the particle shapes is mainly attributed to the motion of the liquid through the particle filling. An experimental comparison of spheres and tetrapods as solid particles in a solid-liquid filled PD can be seen in Fig. 14. The tetrapods provide an evident advantage over simple spheres in the damping behaviour, which shows potential for further investigation. To study the effects leading to the observed advantages, detailed insights into the PD filling are advantageous. Therefore, the established SPH-DEM simulations are adapted for non-convex polyhedra, as it is described in [13]. In Fig. 15 (left), the velocity of the partially liquid-filled PD with

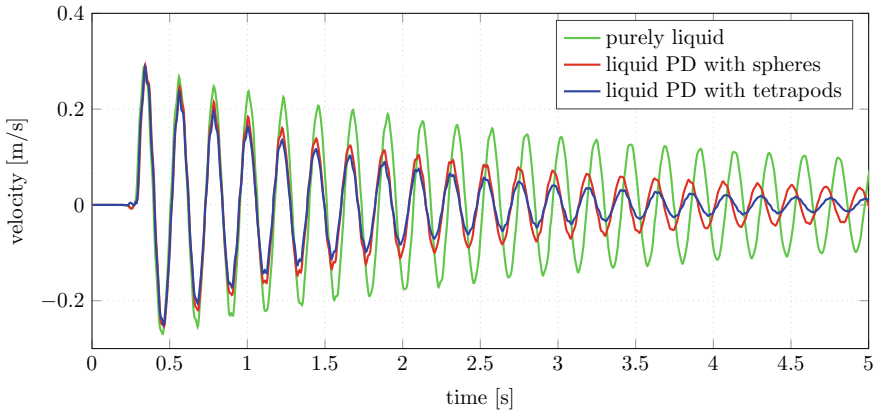


Fig. 14 Comparing solid particles with different shapes and additional liquid. The tetrapod shaped particles perform better compared to spherical particles or pure liquid. The overall mass is kept constant at all cases

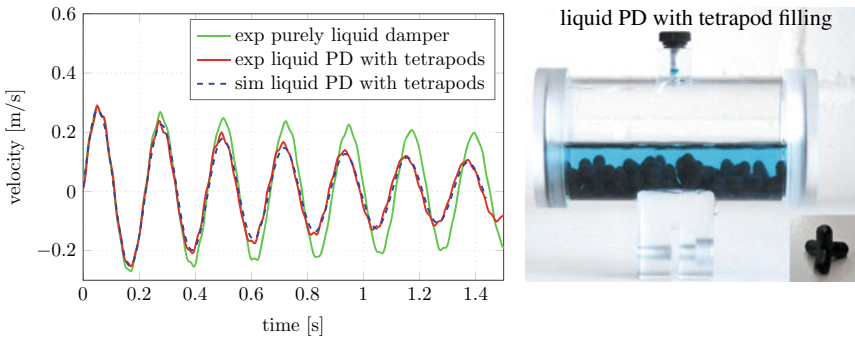


Fig. 15 The red line represents the container velocity measured during laboratory experiments for the liquid-filled PD case with tetrapods. The blue dotted line represents the container velocity predicted by coupled SPH-DEM simulation. An excellent agreement between experiments and simulations are observed

tetrapod shapes, measured during experiments and predicted by coupled SPH-DEM simulation is compared. In order to better understand the effect of solid particles, the velocity for a damper filled purely with a liquid measured during experiments is also plotted in Fig. 15 (left). Macroscopically seen, there is a good agreement between simulations and experiments, showing that coupled SPH-DEM simulations can adequately model the dynamics involved in a partially liquid-filled particle damper, also for the case of non-convex polyhedra as solid particles. It can be clearly seen, that the velocity decay is faster for the case with both liquid and solid filling, than for the purely liquid filled case, confirming the previous experimental findings. The gained

insights through simulations allow for a more detailed investigation of the underlying damping effects.

The observed improvements can, therefore, be explained as follows. First, the solid particles due to the hydraulic forces applied by the liquid, remain agile even under lower vibration amplitude, thereby leading to more effective collisions and in turn more energy dissipation. Secondly, the liquid is squeezed between two approaching solid particles leading to shearing of liquid layers. This ultimately results in more energy dissipation. In this case, the non-convex tetrapod particles behave effectively as obstacles to waves created by liquid motion. These general findings concerning the filling of PDs also raise an additional research question. What should the solid-liquid fill ratio be in order to maximize the dissipation rate? In order to gain further insights regarding this question a numerical investigation is performed. In this numerical study the number of tetrapod solids are varied in three stages (0, 40, 60 solids) while the amount of liquid is kept at a constant volume of 30 ml. By this way, the solid-liquid ratio is implicitly varied. For this study, the density of each solid tetrapod particle is chosen to be 7850 kg m^{-3} . While setting up the simulations, compensation masses were added to the system mass so that all the configurations have the same static mass.

In Fig. 17 (left) the simulated velocity decay for different solid-liquid fill ratios is compared and the corresponding average logarithmic decay rate is visualized in Fig. 17 (right). Moreover, increasing the number of solids particles seem to substantially increase the decay rate. As the number of solid particles, also in the presence of a liquid, governs the number of solid particle collisions. Additionally, the liquid flow is observed to be more fierce with increase in the number of solid particles, leading to even more kinetic energy dissipation. This effect is highlighted by calculating the logarithmic decay. The most significant step is from a purely liquid filling to the use of tetrapods and additional liquid. But also the increase of particle numbers clearly shows to improve the damping effect. In Fig. 16 the simulation of the tetrapod and liquid filled particle damper is illustrated. It can be seen, that the tetrapods lead to a higher pressure in the fluid when the it sloshes through them, resulting in an increased damping effect. For more details of the simulation, see [14].

3 Obstacle Grids

An additional approach to increase damping in PDs are obstacle grids. These grids improve the interaction between the PD container and the particles by preventing the clustering of particles. This increases the energy transferred from the container to the particle filling and allows for greater particle movement. Obstacle grids, therefore, are especially advantageous for systems under forced excitation. For experimental investigations of this approach, a different testbench is introduced. The main difference lies in the change to a forced excitation through an electromagnetic shaker. The laboratory apparatus consists of a horizontally mounted steel beam of dimensions $540 \text{ mm} \times 20 \text{ mm} \times 2 \text{ mm}$, which is rigidly clamped on one side.

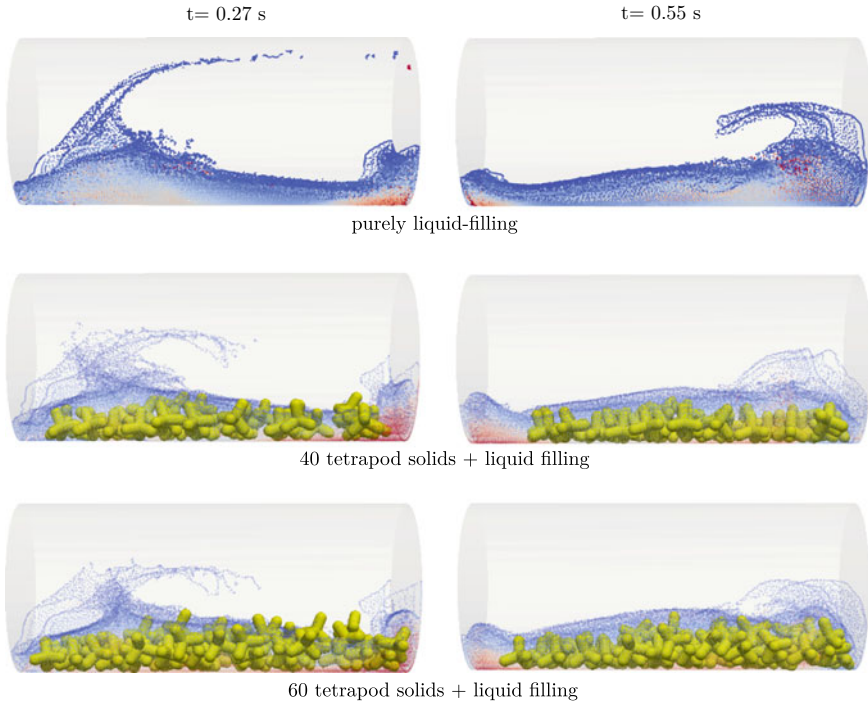


Fig. 16 The motion of damper contents visualized for (top row) purely liquid-filled damper, (middle row) 40 tetrapod solid + liquid and (bottom row) 60 tetrapod solids + liquid, at two different time instances. In all cases, the fluid is visualized as coloured balls, where the colour coding visualizes pressure from low (red) to high (blue)

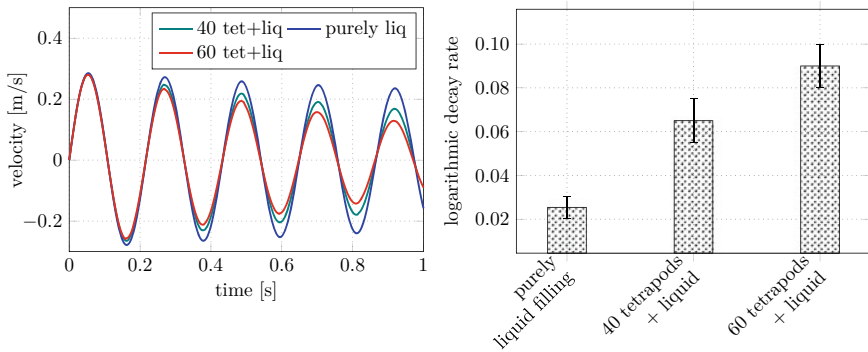


Fig. 17 (left) The velocity of the damper container for various solid-liquid fill ratios is compared. (right) The average logarithmic decay rate, computed at the end of every cycle, is visualized with respect to different solid-liquid fill ratios

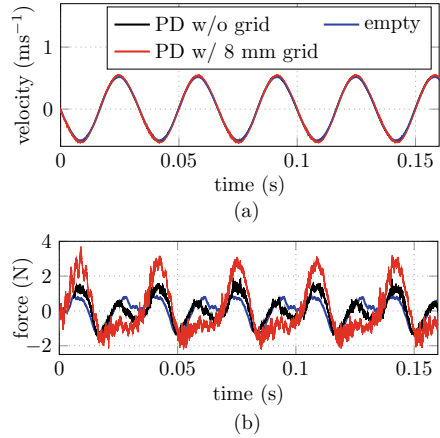
The PD enclosure, weighing 58.8 g, is a transparent acrylic box of inner dimensions 35 mm × 35 mm × 20 mm, which is fixed to the side of the beam. This PD enclosure is filled with steel spheres of 2 mm diameter. The total mass of the spherical particles was kept constant at 0.03 kg throughout this investigation, which corresponds to 1880 spheres. The uniform obstacle-grid used for this investigation has several cells, each having a gap volume corresponding to a cube of size 8 mm. The size of each of these cubes is a characteristic dimension of the obstacle-grid and will be referred to as the cell-size of the obstacle-grid. The uniform obstacle-grid used in the experiments was manufactured using a Formlabs Form 2.0 Stereolithography (SLA) 3D printer. Additional information about the experimental setup can be found in [15]. In order to characterize dissipation in the system, a procedure similar to the one described in [16] is followed. In this procedure a dissipation parameter η is computed for a structure at resonance as the ratio of the measured average power dissipated over time period T and half the square of the absolute input velocity amplitude. The dissipation parameter η has a unit of Ns m^{-1} . Similar dissipation parameters have been used in [17, 18] for characterizing PDs. The dissipation parameter for a sinusoidal motion can be written as

$$\eta = \frac{\frac{1}{T} \int_t^{t+T} \dot{y} f_e dt}{\frac{A^2 \omega^2}{2}}. \quad (2)$$

Here, A is the amplitude, ω is the frequency of the sinusoidal motion function. Moreover, f_e is the force applied on the PD enclosure due to particle interactions in the direction of oscillation. It is to be noted, that due to the discrete nature of the particle interactions the dissipated energy measurement varies over time. In order to take this into account, the dissipation measure for each PD configuration is calculated by averaging over several oscillation cycles. Throughout this investigation, the structure was excited at varying amplitudes at its second resonance frequency, in this case at 27 Hz and correspondingly a time period T of 0.037s. The second mode of the beam allows positioning of the PD at a precise location where there is minimum rotation and nevertheless maintain large driving amplitudes.

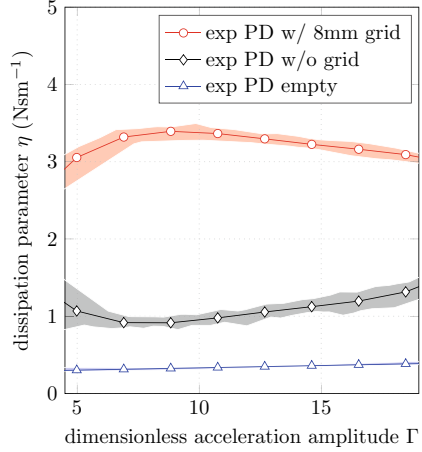
In Fig. 18, the driving forces and resulting forces on the container are shown for such a system containing of a leaf spring with mounted PD. The damping performance of three different configurations is experimentally compared. The first configuration consists of an empty PD enclosure without particles or an obstacle-grid. The empty PD configuration allows the quantification of the dissipation present due to intrinsic material behavior and other external effects. By this way, the additional energy dissipation contribution purely due to particle interactions can be better understood. The second configuration consists of a conventional PD solely filled with solid particles. In the third configuration, the damper contains in addition to solid particles a deliberately introduced 3D printed obstacle-grid. In order to ensure a fair comparison between all the damper configurations, compensation masses were added during the laboratory experiments, so that all the configurations have the same static mass, measured using a weighing scale. A comparison of typical experimental lines,

Fig. 18 Typical measurement obtained from laboratory experiments. **a** Driving velocity of the PD enclosure for the three configurations. **b** Container forces. It can be seen that the container forces are higher in the case where the PD is equipped with an obstacle-grid, indicating more dissipation



showcasing the velocity and force measurements, of the three damper configurations is shown in Fig. 18. In general it can be said that all the waveforms, irrespective of the configuration, are periodic indicating that a steady-state is being reached. Even though the velocity signal seems to be nearly sinusoidal, the force signal is complex, due to the presence of higher modes of the clamped beam. It can be seen in Fig. 18b, that for the same input velocity, the impedance forces (red curve) measured for a PD with an obstacle-grid seems to be drastically higher, indicating higher energy dissipation in this case compared to the other configurations. Similarly, the dissipation parameter η computed using Eq. 2 for all the PD configurations is presented in Fig. 19 as a function of the dimensionless acceleration amplitude $\Gamma = A\omega^2/g$, where g is the acceleration due to gravity. The translucent bands around the curves represent the variance present in several experiments for the measured dissipation parameter. It can be seen, that due to the absence of particles, the variance present in the empty PD case is negligible compared to other configurations. As a consequence, the dissipation in the empty PD case (blue line with triangle markers), which occurs due to intrinsic structural damping, is far lower compared to other configurations. A higher dissipation rate is observed for the case with particles than for the empty case. It is also seen in Fig. 19 (black line with diamond markers), that increasing the acceleration amplitudes seems to steadily increase dissipation, at least starting from $\Gamma = 6$, for the conventional PD case. For lower acceleration levels, between $\Gamma = 3$ and $\Gamma = 6$, the measured dissipation for the conventional PD case seems to have high variance. This is probably due to the very noisy force signals measured during these experiments. Perhaps the most interesting aspect of Fig. 19 is the dissipation behavior of a PD with a deliberately introduced obstacle-grid. The dissipation rate for a PD with obstacle-grids irrespective of the acceleration amplitude clearly outperforms the conventional PD without an obstacle-grid. This is arguably due to the increased particle activity and relative motion of the particles leading to more effective collisions and thereby increasing energy dissipation. Moreover, at an acceleration amplitude of $\Gamma = 10$ the dissipation rate for the PD with obstacle-grid is

Fig. 19 Dissipation parameter for all the PD configurations as a function of the dimensionless acceleration amplitude $\Gamma = A\omega^2/g$. The translucent bands around the curves represent the variance observed during the experimental trials. The deliberate introduction of an obstacle-grid drastically increases dissipation



observed to reach an optimum. Additional information about the simulation model and the contact detection algorithm used can be found in [15].

The comparison of the resulting simulations with the previously conducted experiments in Fig. 20 (b) shows good agreement. This is the case for both configurations with and without the use of an obstacle grid. The previously mentioned increase in particle motion through the grid can clearly be observed in the simulation visualizations namely subfigures (d) and (e) in Fig. 20. This also highlights again the useful additional insights into the PD provided through numerical simulations. A more detailed discussion of these results and additional visualisations of the simulation data can also be found in [15].

Next, a numerical study is set up to investigate the effect of cell-size on the damping performance of a PD with an obstacle-grid. For this purpose, obstacle-grid geometries with two different cell-sizes, namely 5 mm and 8 mm, are investigated, as depicted in Fig. 21. In order to ensure a fair comparison, the PD is filled with the same amount (0.03 kg) of spherical steel particles for both simulation scenarios. In order to predict the effect of obstacle-grid cell size several simulations are performed. During each simulation, the PD equipped with an obstacle-grid of a particular cell-size is driven with a sinusoidal velocity at a constant frequency of 27 Hz for 5 cycles. The resulting container forces accumulated due to particle interactions are recorded at every numerical time step and are utilized to compute an average dissipation rate for each cycle according to Eq. 2. This procedure is performed for both obstacle-grid sizes and for several acceleration amplitudes Γ . The results are reported in Fig. 21c. As seen in Fig. 21c, the dissipation rate predictions for the two configurations are significantly different, even though all the parameters except the obstacle-grid cell-size are identical. Therefore, the cause of the observable difference in dissipation rate must be entirely due to the geometry of the obstacle-grid. It can be observed, that for both cases a clear peak in dissipation rate is observed at a specific acceleration amplitude. The peak dissipation rate predicted for a PD with 8 mm grid is higher at

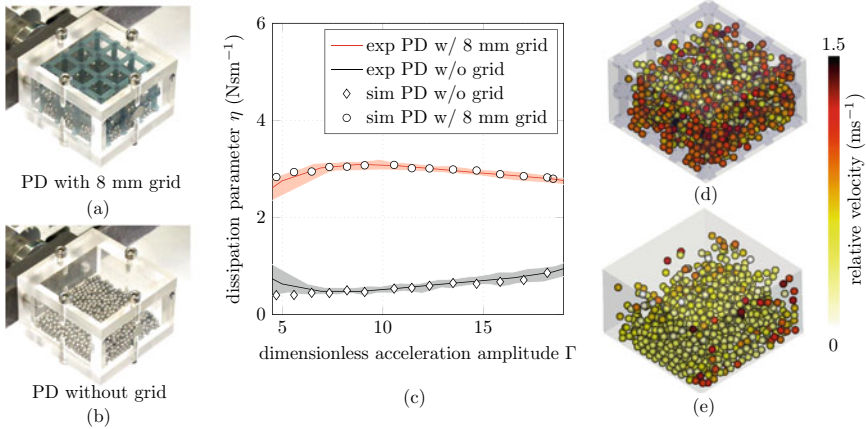


Fig. 20 **a** and **b** show the PD configurations tested during the laboratory experiments. **c** Comparison of the dissipation parameter predicted using DEM simulations and measured during lab experiments. A good agreement between experiments and simulations is observed. Visualizations of the particle motion predicted by DEM simulations **d** with and **e** without an obstacle-grid for $\Gamma = 10$. Here, the obstacle-grid **d** is made translucent for visualization purposes. Particles attain far higher relative velocities for the case with a obstacle-grid than without it

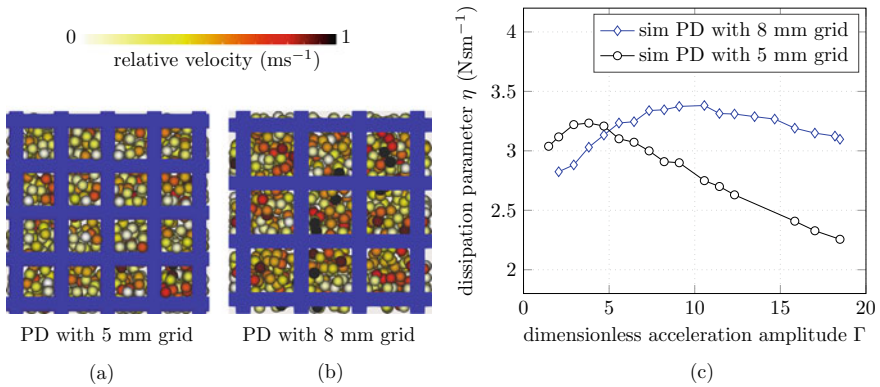


Fig. 21 A numerical study compares the damping performance of PDs with obstacle-grids of two different cell-sizes namely **a** 5 mm and **b** 8 mm. In this simulation, both configurations were subjected to $\Gamma = 10$ and the color gradient represents the relative velocity of the solid particles with respect to the PD container. **c** Results show the noticeably distinct dissipation rates predicted for the two cell-sizes at various acceleration levels. The dissipation rate for the PD with 5 mm grid peaks at a different acceleration level compared to the PD with 8 mm grid. This shows, that the obstacle-grid cell size plays a crucial role in the design of PDs with obstacle-grids

3.38 N s m^{-1} than the peak dissipation of a PD with 5 mm grid which is found to be 3.23 N s m^{-1} . Moreover, the acceleration level at which the dissipation rate peaks is higher at $\Gamma = 10$ for PD with 8 mm grid than for PD with 5 mm grid at $\Gamma = 4$. This indicates that the cell size could be used as an additional tuning parameter to control the damping performance of PDs equipped with an obstacle-grid. More interestingly, after the maximum dissipation is reached, the rate at which the dissipation parameter decreases for the case of a PD with 5 mm grid is much steeper than for the PD with 8 mm grid. This shows that the PD with 8 mm grid seems to be less sensitive, in other words more robust, to changes in the driving acceleration level.

4 Broadband Properties

To study the broadband damping properties of a PD, a weakly damped frame structure as shown in Fig. 22 is designed and build. This frame structure exhibits multiple vibration modes even in the lower frequency range. When excited with a shaker, the

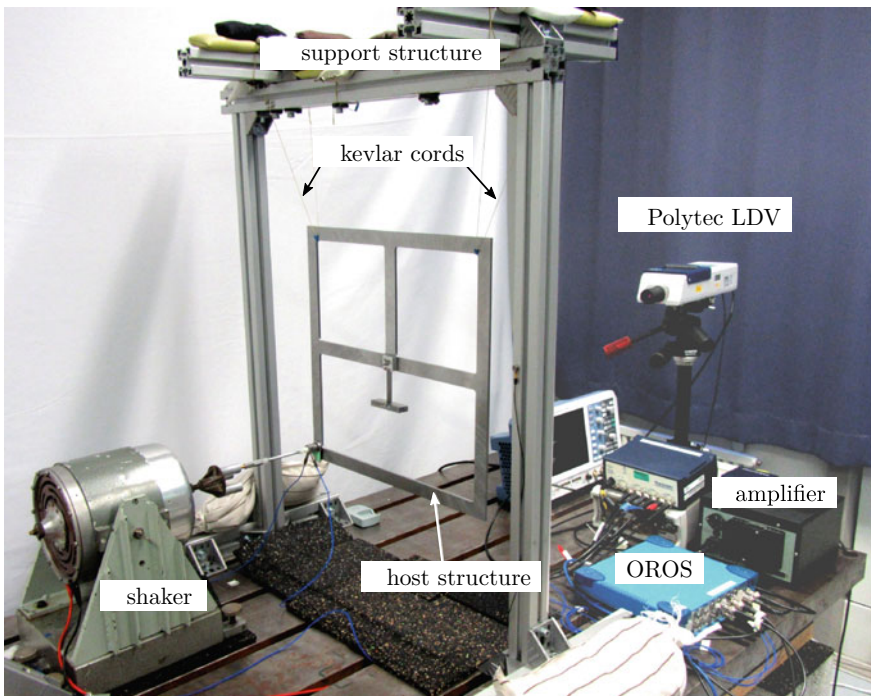


Fig. 22 Lab apparatus consisting of the host structure hung using kevlar cords. The host structure is excited using an electrodynamic shaker. A Laser Doppler Vibrometer is used to measure the structural response

frequency response of the host structure with a PD allows a systematic investigation of the broadband damping effect of PDs. In Fig. 22, the surrounding lab setup used for the experiments is also shown. The host structure is suspended by kevlar cords to replicate a free-free boundary condition. This gives the opportunity to study the dynamics of the structure independently from clamping to a surrounding suspension. The host structure is excited using an electromagnetic shaker Elektro-Mechanik Schmid SW100, which is driven by a power amplifier Brüel & Kjær Type 2706. The driving signal for the shaker is controlled using a Tectronix AFG2022B signal generator. A PCB 288D01 impedance sensor situated between the shaker and the host structure is used to measure the force and acceleration at the forcing point (input). The forces and accelerations at the input vary, but are in a range up to 55 N and 40 ms^{-2} peak values, respectively. For more information about the structure used, as well as, detailed pictures of the experimental setup refer to [21].

4.1 Comparison with Tuned Mass Damper

In order to investigate the influence of a PD on the host structure, the steady state frequency response functions (FRFs) of three different configurations are measured. The three configurations are: host structure with an added ballast mass (BM), host structure with a tuned mass damper (TMD) and host structure with a PD. The ballast block is in the same location as the PD and its mass is equal to the static mass of the particle damper. The TMD also has the same static mass and is chosen for comparison as it is a common device for suppressing unwanted vibrations in technical applications. Also, considering broadband properties, it poses a contrasting concept as it only works well within a narrow frequency band around the tuning frequency. The FRFs for the three configurations are generated by driving the shaker with a frequency sweep signal from 25 to 100 Hz. To make sure that a quasi-steady state is reached, a relatively long frequency sweep time of 375 s is chosen. Figure 23 shows the frequency response of the host structure with a TMD, with a PD and with a BM. It is clearly seen that near the design frequency of 60 Hz, the TMD provides superior vibration suppression compared to a PD. This behaviour is expected, because a TMD works by introducing a vibration node at the point of attachment to the host structure exactly at design or operating frequency. Therefore, a conventional TMD actually does not directly dissipate the vibrational energy but rather transfers the energy to the vibration of the attached auxiliary mass. The movement of this mass functions as a kinetic energy reservoir and also leads to dissipation through material damping of the deflected TMD beam, friction in the joints, etc.. Furthermore, a TMD introduces an additional degree of freedom to the host structure and thus, adds additional resonance frequencies. This is clearly seen in the additional resonance peak at 70 Hz for the case where the host structure is fitted with a TMD, see the blue dashed curve in Fig. 23.

Additionally, the introduction of a TMD lowers the natural frequencies of the reference host structure that are below the design frequencies. For instance, the nat-

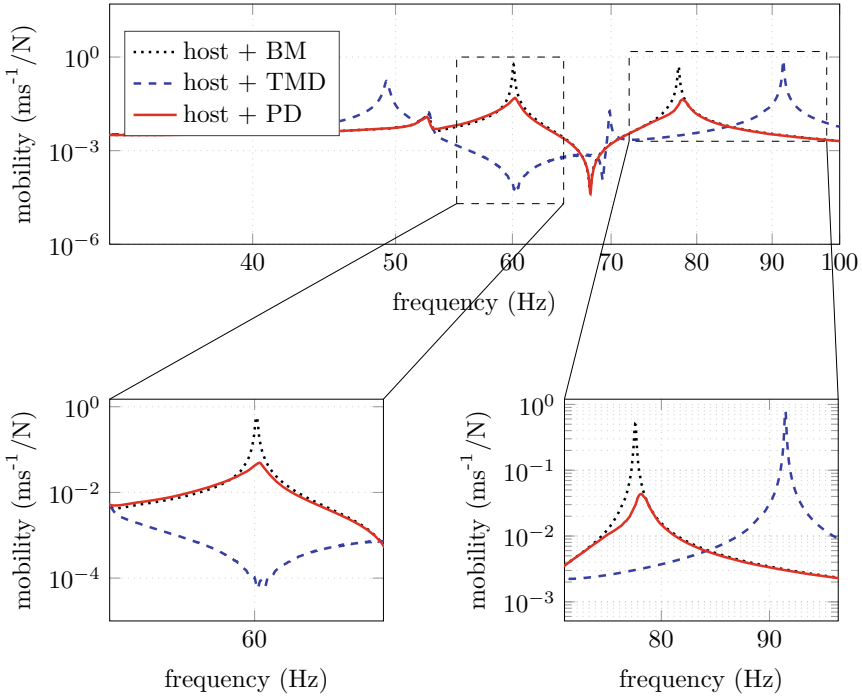


Fig. 23 Experimental frequency response of the host structure with a BM, TMD and PD. Near the design frequency of 60 Hz, the TMD provides superior vibration attenuation compared to a PD. However, the PD provides considerable vibration damping at multiple resonance frequencies at the same time

ural frequency at 60 Hz is now lowered to 45 Hz. On the other hand, the resonance frequencies of the reference host structure that are higher than the design frequency, for instance the frequency at 80 Hz, are raised with the introduction of a TMD, see Fig. 23 for high frequencies. On the whole, the TMD, even though it does a very good job in reducing vibration near the design frequency of 60 Hz, drastically alters the frequency response of the host structure and creates trouble at other frequencies. Another aspect of the TMD is, that its vibration attenuation property is highly sensitive to changes in stiffness and mass of the auxiliary system. In other words, changes in the TMD configuration, for instance due to fatigue, lead to a detuning of the TMD which could result in a sudden unwanted increase in vibrations. Therefore, care has to be taken when designing a TMD and it should only be used for a system that is subjected to a constant frequency excitation.

On the other hand, PDs provide considerable vibration damping not only at 60 Hz but also at other frequencies. Unlike a TMD, PDs due to inter particle collisions and friction, actually dissipate the vibrational energy of the host structure and convert it to other energy forms (for instance heat). As seen in Fig. 23, the energy dissipation in the PD is relatively insensitive to the excitation frequency and highly sensitive to

the external motion at the attachment point. Consequently, the PD affects the host structure only where the host structure shows high vibration amplitudes and induces no alternation elsewhere, see Fig. 23.

4.2 Towards Quantifying Broadband Dissipation

The experimental investigations shown have opened up two crucial questions which are yet to be addressed. To what extent does a particular damping device influence the frequency response of the host structure? Moreover, how can a damping device be rated according to its broadband damping property? In order to answer these questions, two additional quantities are introduced.

Firstly, the dynamic influence factor S_{dev} is introduced, which is the ratio of the mobility of the host structure with the damping device to the mobility of the host structure with a ballast block having the same static mass of the device. The factor S_{dev} is defined as

$$S_{\text{dev},f} = \frac{M_{\text{dev},f}}{M_{\text{ref},f}}, \quad (3)$$

where $M_{\text{dev},f}$ is the mobility (velocity/force) of the structure with the damping device at the frequency f and $M_{\text{ref},f}$ is the mobility of the host structure with an equivalent mass block. The factor S_{dev} helps to quantify the effect of the particular damping device on the host structure. For instance, a high dynamic influence (greater than 1) indicates vibration amplification and a low value (smaller than 1), indicates vibration reduction. The dynamic influence factor S_{dev} applied to the investigated host structure with a PD and a TMD is shown in Fig. 24. It can be seen that the dynamic influence factor for the TMD has a very low value near the design frequency of 60 Hz, meaning vibration attenuation is only observed around the design frequency. Apart from the design frequency, especially at 49 Hz, 68 Hz, 91 Hz frequencies, the dynamic influence factor for the TMD case has high positive values, indicating even a vibration amplification at these frequencies, i.e. a worsening of the dynamic behaviour. From a practical point of view these vibration amplifications observed only in the TMD case are disadvantageous. This is because the TMD, apart from providing the vibration attenuation at the design frequency, fundamentally alters the frequency response of the host structure elsewhere and might even make it worse than that of the undamped structure.

Interestingly, the dynamic influence for the PD case is relatively smooth compared to the TMD case. The S_{PD} for the PD case attains values smaller than one (meaning vibration reduction) at frequencies where the host structure exhibits high vibration amplitudes. Usually, the value of S_{PD} is close to one. This means that the PD is a passive damping device which smoothens the resonance peaks without fundamentally altering or shifting the natural frequencies of the host structure.

Secondly, to analyse the broadband damping property of a device, another quantity namely the mean influence deviation σ_{dev} is introduced. The deviation σ_{dev} is defined

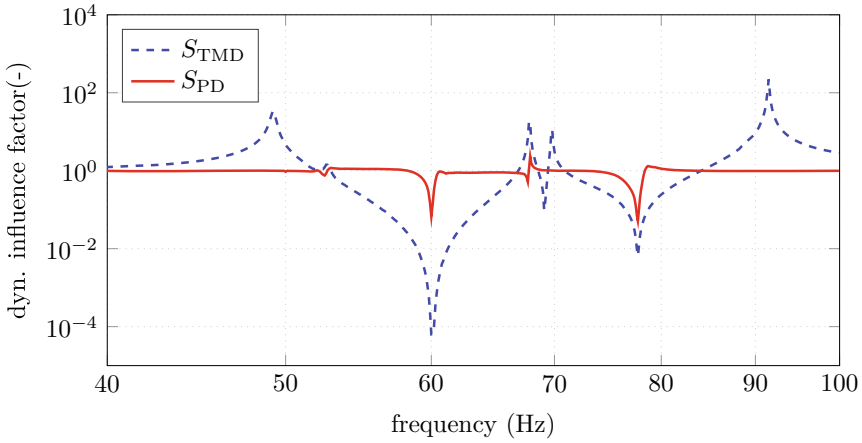


Fig. 24 Dynamic influence factor computed for the host structure equipped with a PD and a TMD. The S_{PD} shows that the PD influences the host structure only for high vibration amplitudes, whereas S_{TMD} shows that the TMD fundamentally alters the frequency response of the host structure

as the squared deviation of the dynamic influence factor from its mean behaviour of a particular damping device. This can be defined as

$$\sigma_{dev,f} = (S_{dev,f} - \bar{S}_{dev})^2, \tag{4}$$

where \bar{S}_{dev} is the average dynamic influence factor of the host structure equipped with a particular damping device. In other words, σ_{dev} indicates the extent to which a device deviates from its mean response over frequency. A high value of σ_{dev} means, that the device changes its behaviour to a large extent. A perfect broadband damping device would have a value of zero, even though such a device would be impractical. Figure 25 shows the curves for σ_{TMD} and σ_{PD} computed for the host structure equipped with a TMD and PD, respectively. It is clearly seen that the deviation σ_{PD} for the PD case has a much lower numerical value over the entire frequency range when compared to a TMD. This means that the behaviour of a PD does not drastically deviate from its mean performance compared to a TMD. For the TMD case it can be seen that the vibration amplification around 49 Hz and 91 Hz are prominent in the influence deviation as well. However the attenuation around 60 Hz leads to no observable peak. This is due to numerically small numbers of S_{TMD} from which the constant \bar{S}_{dev} is subtracted. The formulation of $\sigma_{dev,f}$ in Eq. 4 especially highlights positive deviation from \bar{S}_{dev} which leads to undesired vibration amplification caused by the damping device.

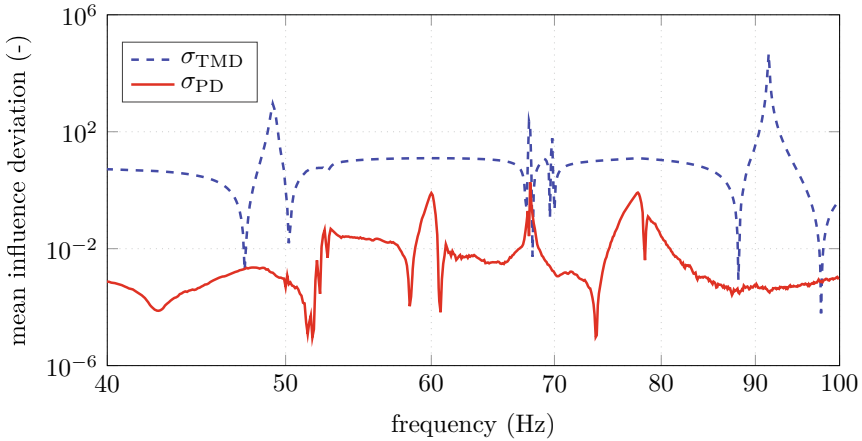


Fig. 25 Mean influence deviation computed for the host structure equipped with a TMD and a PD. The σ_{PD} has smaller values compared to σ_{TMD} indicating that the PD does not drastically deviate from its mean behaviour compared to a TMD

Therefore, the value S_{dev} provides quantitative insights on the extent to which a device influences the host structure and σ_{dev} provides insights regarding the broadband damping property of a damping device. So, S_{dev} and σ_{dev} together provide the right tools to quantitatively investigate damping devices or parameter changes systematically.

5 Conclusion

The emphasis of this research project was the improvement of PDs and their applicability. Therefore, several PD concepts were analysed through experiment and simulation. To improve the damping properties of PDs, the concepts investigated included, e.g., additional liquid, complex particle shapes, and obstacle-grids. These variations on PD fillings provided significant enhancement of damping under various loading conditions. Especially the combined approach of simulations supported by meaningful laboratory experiments allowed for a targeted investigation of the different concepts. The simulations allow detailed insights into the behaviour of the PD fillings and the experiments ensure the approximations made for the simulation model are realistic and yield good agreement with measured data. The ability to examine the particles during simulations in detail for every timestep is of great benefit for the understanding of the damping processes within the PD. This is especially important for a targeted design improving the applicability of PDs for a special use case. The general applicability was improved in this project by investigating damping properties over a wide frequency range with the help of test structures with dynamical

behaviour relevant for industrial applications. In this context, the PD was also directly compared to a conventional TMD which is already widely used in technical applications. In this research project, the usage of PDs for targeted damping in structures and technical applications showed to be feasible and beneficial. Further research in this field seems promising to further improve the applicability of PDs and make them usable in various application fields over wide ranges of frequency and loading amplitudes. Enabling the industry to use PDs as standard damping devices seems of great interest in many fields.

Acknowledgements This research has received funding from the German Research Foundation (DFG) within the priority program SPP 1897 “Calm, Smooth and Smart: Neuartige Schwingungsbeeinflussung durch gezielt eingesetzte Dissipation” project EB195/25-1/2 “Partikeldämpfer—Schwingungsbeeinflussung durch verteilte Dissipation über komplexe Partikelformen” (project number 315008544). This support is highly appreciated.

References

1. Panossian, H.: Structural damping enhancement via non-obstructive particle damping technique. *J. Vib. Acoust.* **114**, 101–105 (1992)
2. Harris, C.M., Crede, C.E.: *Shock and Vibration Handbook*. McGraw-Hill, New York (1976)
3. Heckel, M., Sack, A., Kollmer, J.E., Pöschel, T.: Granular dampers for the reduction of vibrations of an oscillatory saw. *Phys. A* **391**(19), 4442–4447 (2012)
4. Xiao, W., Huang, Y., Jiang, H., Lin, H., Li, J.: Energy dissipation mechanism and experiment of particle dampers for gear transmission under centrifugal loads. *Particology* **27**, 40–50 (2016)
5. Ma, C., Lu, Z., Wang, D., Wang, Z.: Study on the damping mechanisms of a suspended particle damper attached to a wind turbine tower. *Wind Struct.* **33**(1), 103–114 (2021)
6. Veeramuthuvel, P., Shankar, K., Sairajan, K.K.: Application of particle damper on electronic packages for spacecraft. *Acta Astronaut.* **127**, 260–270 (2016)
7. Tomlinson, G., Pritchard, D., Wareing, R.: Damping characteristics of particle dampers - some preliminary results. *Proc. Inst. Mech. Eng. C J. Mech. Eng. Sci.* **215**(3), 253–257 (2001)
8. Marhadi, K.S., Kinra, V.K.: Particle impact damping: effect of mass ratio, material, and shape. *J. Sound Vib.* **283**, 433–448 (2005)
9. Liu, W., Tomlinson, G.R., Rongong, J.A.: The dynamic characterisation of disk geometry particle dampers. *J. Sound Vib.* **280**, 849–861 (2005)
10. Pasimodo - Particle Simulations Software. www.itm.uni-stuttgart.de/software/pasimodo (last accessed on 07-06-2020)
11. Gnanasambandham, C., Schönle, A., Eberhard, P.: Investigating the dissipative effects of liquid-filled particle dampers using coupled DEM-SPH methods. *Comput. Particle Mech.* **6**, 257–269 (2019)
12. Gnanasambandham, C., Eberhard, P.: Predicting the influence of an added liquid in a particle damper using coupled SPH and discrete element method. *PAMM Proc. Appl. Math. Mech.* **17**, 31–32 (2018)
13. Gnanasambandham, C., Eberhard, P.: Investigating the effect of complex particle shapes in partially liquid-filled particle dampers using coupled DEM-SPH Methods. *PAMM Proc. Appl. Math. Mech.* **19** (2019)
14. Gnanasambandham, C., Eberhard, P.: Modeling a partially liquid-filled particle damper using coupled Lagrangian methods. In: *International Centre for Numerical Methods in Engineering (CIMNE), Barcelona* (2019)
15. Gnanasambandham, C., Fleissner, F., Eberhard, P.: Enhancing the dissipative properties of particle dampers using rigid obstacle-grids. *J. Sound Vibrat.* **484**, 115522 (2020)

16. Yang, M.; Lesieutre, G.; Hambric, S.; Koopmann, G.: Development of a design curve for particle impact dampers. In: Proceedings of the 11th Annual International Symposium on Smart Structures and Materials, pp. 450–465 (2004)
17. Salueña, C., Pöschel, T., Esipov, S.E.: Dissipative properties of vibrated granular materials. *Phys. Rev. E* **59**, 4422–4427 (1999)
18. Wong, C., Daniel, M., Rongong, J.: Energy dissipation prediction of particle dampers. *J. Sound Vib.* **319**, 91–118 (2009)
19. Ericson, C.: *Real-Time Collision Detection*. Elsevier, Amsterdam (2005)
20. Klosowski, J., Held, M., Mitchell, J., Sowizral, J.: Efficient collision detection using bounding volume hierarchies of K-Dops. *IEEE Trans. Visual Comput. Graphics* **1**, 21–37 (1998)
21. Schönle, A.; Gnanasambandham, C., Eberhard, P.: Broadband damping properties of particle dampers mounted to dynamic structures. *Exper. Mech.* (2022)